Journal of Biological Dynamics, 2013
Vol. 7, Suppl. 1, 4–20, http://dx.doi.org/10.1080/17513758.2013.789562

Taylor & Francis
Taylor & Francis Group

A numerical approach for investigating the stability of equilibria for structured population models

Dimitri Breda[a]*, Odo Diekmann[b], Stefano Maset[c] and Rossana Vermiglio[a]

[a]*Department of Mathematics and Computer Science, University of Udine, via delle Scienze 208, I-33100 Udine, Italy;* [b]*Department of Mathematics, University of Utrecht, Budapestlaan 6, PO Box 80010, 3508 TA Utrecht, The Netherlands;* [c]*Department of Mathematics and Computer Science, University of Trieste, via Valerio 12, I-34127 Trieste, Italy*

(*Received 15 May 2012; final version received 19 March 2013*)

We are interested in the asymptotic stability of equilibria of structured populations modelled in terms of systems of Volterra functional equations coupled with delay differential equations. The standard approach based on studying the characteristic equation of the linearized system is often involved or even unattainable. Therefore, we propose and investigate a numerical method to compute the eigenvalues of the associated infinitesimal generator. The latter is discretized by using a pseudospectral approach, and the eigenvalues of the resulting matrix are the sought approximations. An algorithm is presented to explicitly construct the matrix from the model coefficients and parameters. The method is tested first on academic examples, showing its suitability also for a class of mathematical models much larger than that mentioned above, including neutral- and mixed-type equations. Applications to cannibalism and consumer–resource models are then provided in order to illustrate the efficacy of the proposed technique, especially for studying bifurcations.

Keywords: numerical equilibrium analysis; structured populations; Volterra functional equations; delay differential equations; infinitesimal generator

AMS Subject Classifications: 34L16; 37M20; 65L07; 92D25

1. Introduction

To better describe real phenomena, more complex mathematical models have been developed over the years. As a consequence, sharper mathematical tools and accurate and efficient numerical methods are needed to analyse them. In many different scientific disciplines, such as physics, biology, economics, engineering and chemistry, the modern way to conduct research makes use of numerical simulations too, to provide a deeper insight into the phenomena. Our aim is to show how suitable numerical methods can advance the theoretical analysis of population dynamical models.

In particular, we are interested in the stability analysis of equilibria of structured population models, as those recently proposed, for example, in [10,11,18,19]. Such models take the form of Volterra functional equations (VFEs) coupled with delay differential equations (DDEs). In [10], the stability and instability parts of the principle of linearized stability and the Hopf bifurcation theorem have been derived through the sun–star approach for either VFEs or VFEs coupled with

*Corresponding author. Email: dimitri.breda@uniud.it
Author Emails: O.Diekmann@uu.nl; maset@units.it; rossana.vermiglio@uniud.it

DDEs. The fundamental theoretical results state that the spectral properties of the infinitesimal generator (IG) of the linearized semigroup generically determine the stability or instability of an equilibrium and that the (point-)spectrum of the IG is given by the roots of the characteristic equation. Despite this theoretical support, the analysis after the linearization is often rather complex, and accordingly, numerical methods are needed.

In the last decade, a direct technique for computing (part of) the eigenvalues of the IG has been proposed, based on its discretization by a pseudospectral approach. The eigenvalues of the resulting matrix are taken as approximations of the exact spectrum. This methodology, that here we call the IG approach, has been developed and applied for the stability analysis of equilibria of different classes of differential equations: delay [2], neutral-delay and mixed-type [3], partial differential equations of the reaction–diffusion type with delay in the reaction term [7], as well as age-structured populations and epidemic models [5,13]. The IG approach does not compute roots of the characteristic equation, which could be difficult and could give rise to an ill-conditioned problem: basically, it can suffer from the conditioning problems that already arise in the computation of the roots of a polynomial [23] (these are indeed better computed as eigenvalues of corresponding matrices). Moreover, its outstanding feature is the so-called spectral accuracy, that is, convergence of infinite order of the computed eigenvalues to the exact ones. This translates into rather fast and efficient algorithms that can be employed to perform a robust analysis of the model for varying parameters, producing, for example, bifurcation diagrams and stability maps [6].

It is worth mentioning that in the context of DDEs (especially in the control field), there are also other approaches to approximate or locate the characteristic roots (see e.g. [12,14,17,22]). In particular, both the methods adopted in [12,14] could be extended in principle to tackle the problem we consider here. Also, we refer the reader to [16] for the classical literature on the approximation of generators of semigroups, even though it does not furnish precise estimates [15] whence it is requested to exploit the special structure of the problem and of the approximation [2].

In this paper, we extend the potential of the IG approach to physiologically structured populations modelled as coupled VFEs/DDEs. This requires to combine the method for DDEs [2] and the alternative idea used for age-structured populations [5], a necessity due to the different types of nonlocal conditions characterizing the domain of the relevant IGs. The resulting algorithm, beyond being suitable for systems of coupled VFEs/DDEs, is shown to approximate correctly the spectrum of more general operators, such as those corresponding to neutral and advanced–retarded equations, although in these cases the theoretical results linking such spectra to possible notions of stability are different and out of the scope of the present research.

The work is organized as follows. A brief introduction to the models formulated as coupled VFEs/DDEs is given in Section 2, together with the necessary stability results; next, a prototype is introduced. The IG approach is developed in Section 3, where a concrete algorithm is proposed for the sake of implementation. A discussion on convergence and applicability is the subject of Section 4, where toy examples are used to test the technique. Eventually, in Section 5, we apply the method to analyse the stability of equilibria of a model of cannibalism (a VFE) and of a structured consumer–resource model (a VFE coupled with a DDE, see e.g. [11,19]).

2. Models and stability

To motivate our study, we briefly recall from [11,19] the basic ingredients of a physiologically structured consumer–resource model.

Let $S(t)$ denote the food concentration at time t. Let S_t denote the food history, that is, $S_t(\theta) = S(t+\theta)$ for $\theta \in [-r, 0]$ with the maximum delay r specified below. Assume that $X(a, S_t)$ and $\mathcal{F}(a, S_t)$ are, respectively, the size at age a and time t and the probability to survive till age a at

time t of a consumer that has experienced resource concentration S in the time interval $[t-a,t]$. Let $\beta(X(a,S_t),S(t))$ and $\gamma(X(a,S_t),S(t))$ be the rate of reproduction and food consumption, respectively, of a consumer of age a at time t. Finally, let f be the rate of change of the resource in absence of the consumer. If $b(t)$ denotes the population birth rate of the consumers and $r>0$ is the maximum lifespan under ideal food conditions, the dynamics is described by

$$\begin{aligned} b(t) &= \int_0^r \beta(X(a,S_t),S(t))\mathcal{F}(a,S_t)b(t-a)\,\mathrm{d}a,\\ S'(t) &= f(S(t)) - \int_0^r \gamma(X(a,S_t),S(t))\mathcal{F}(a,S_t)b(t-a)\,\mathrm{d}a, \end{aligned} \tag{1}$$

that is, by a VFE coupled with a DDE. The size X and the survival probability $\mathcal{F}$ can be determined by solving ordinary differential equations once individual growth and mortality rates are given; for further details, see [11,19].

System (1) becomes well posed as soon as suitable histories for b and S are specified. Since the former requires integrability and the latter continuity, it is common to assume that $b(\theta)=\varphi(\theta)$ and $S(\theta)=\psi(\theta)$, $\theta\in[-r,0]$, for given $\varphi\in Y:=L^1([-r,0];\mathbb{R})$ and $\psi\in Z:=C([-r,0];\mathbb{R})$ [11].

Diekmann *et al*. [10] present the stability analysis for VFEs, and by combining with the results developed in the book [9] for DDEs, they also extend it to coupled systems of VFEs and DDEs such as Equation (1). By using the sun–star theory for dual semigroups, they prove the principle of linearized stability and thus show that the stability or instability of an equilibrium of Equation (1) is as a rule determined by the spectral properties of the IG of the linearized semigroup that in the case of Equation (1) is the operator $\mathcal{A}:\mathrm{dom}(\mathcal{A})\subseteq Y\times Z\to Y\times Z$ with action

$$\mathcal{A}(\varphi,\psi)^{\mathrm{T}}=(\varphi',\psi')^{\mathrm{T}}$$

and domain

$$\mathrm{dom}(\mathcal{A})=\left\{(\varphi,\psi)^{\mathrm{T}}\in Y\times Z:(\varphi',\psi')^{\mathrm{T}}\in Y\times Z \quad\text{and}\quad \begin{array}{c}\varphi(0)=l_{11}\varphi+l_{12}\psi\\ \psi'(0)=l_{21}\varphi+l_{22}\psi\end{array}\right\}.$$

The functionals l_{ij} represent the right-hand side of Equation (1) linearized around the equilibrium under consideration. The main results follow.

THEOREM 2.1 *The spectrum of the IG is point spectrum. Every eigenvalue λ has finite algebraic multiplicity and every right half-plane contains at most finitely many eigenvalues. Moreover, λ is an eigenvalue of the IG if and only if it is a root of the characteristic equation*

$$\det\begin{pmatrix}1-l_{11}\mathrm{e}^{\lambda\cdot} & -l_{12}\mathrm{e}^{\lambda\cdot}\\ -l_{21}\mathrm{e}^{\lambda\cdot} & \lambda-l_{22}\mathrm{e}^{\lambda\cdot}\end{pmatrix}=0, \tag{2}$$

and the algebraic multiplicity of λ coincides with its order as root of Equation (2)*.*

THEOREM 2.2 *If all the eigenvalues of the IG have negative real part, then the equilibrium of Equation* (*1*) *is asymptotically stable, whereas if there exists at least one eigenvalue with positive real part, then the equilibrium is unstable.*

To determine the real part of all the roots of the characteristic equation (2) is not an easy task in general, due to the complexity of realistic models (see e.g. [19]). Besides, numerically we may run into ill-conditioning as briefly explained in Section 1. For these reasons, we investigate in Section 3 the IG approach, that is, the computation of finitely many eigenvalues of $\mathcal{A}$ while bypassing the characteristic equation.

Allowing both y and z to be vectors, we consider as prototype the autonomous linear (or linearized) system

$$\begin{aligned} y(t) &= \mathcal{L}_{11} y_t + \mathcal{L}_{12} z_t, \\ z'(t) &= \mathcal{L}_{21} y_t + \mathcal{L}_{22} z_t \end{aligned} \tag{3}$$

for $y_t \in Y := L^1([-r, 0]; \mathbb{C}^{d_1})$ and $z_t \in Z := C([-r, 0]; \mathbb{C}^{d_2})$, where d_1 and d_2 are nonnegative integers. $r > 0$ is the maximum (finite) delay and $\mathcal{L}_{11} : Y \to \mathbb{C}^{d_1}$, $\mathcal{L}_{12} : Z \to \mathbb{C}^{d_1}$, $\mathcal{L}_{21} : Y \to \mathbb{C}^{d_2}$ and $\mathcal{L}_{22} : Z \to \mathbb{C}^{d_2}$ are linear continuous functionals. For later convenience, we rewrite system (3) as

$$\mathcal{M} x_t = 0 \tag{4}$$

for $x_t \in X := Y \times Z$, and with $d := d_1 + d_2$, $\mathcal{M} : X \to \mathbb{C}^d$ unbounded and given by

$$\mathcal{M}\phi = -C_1 \phi(0) - C_2 \phi'(0) + \mathcal{L}\phi, \tag{5}$$

where

$$C_1 := \begin{pmatrix} I_{d_1} & 0 \\ 0 & 0 \end{pmatrix},$$

$$C_2 := \begin{pmatrix} 0 & 0 \\ 0 & I_{d_2} \end{pmatrix}$$

and

$$\mathcal{L} := \begin{pmatrix} \mathcal{L}_{11} & \mathcal{L}_{12} \\ \mathcal{L}_{21} & \mathcal{L}_{22} \end{pmatrix}.$$

The IG $\mathcal{A} : \mathrm{dom}(\mathcal{A}) \subseteq X \to X$ associated to Equation (3) reads

$$\begin{aligned} \mathcal{A}\phi &= \phi', \ \phi \in \mathrm{dom}(\mathcal{A}), \\ \mathrm{dom}(\mathcal{A}) &= \{\phi \in X \mid \phi' \in X \text{ and } \mathcal{M}\phi = 0\}. \end{aligned} \tag{6}$$

The applications of interest often involve multiple discrete and distributed delays, meaning that $\mathcal{L}$ takes the form

$$\mathcal{L}\phi = A^{(0)}\phi(0) + \sum_{k=1}^{p} A^{(k)}\phi(-r_k) + \sum_{k=1}^{p} \int_{-r_k}^{-r_{k-1}} B^{(k)}(\theta)\phi(\theta)\,\mathrm{d}\theta, \tag{7}$$

with $-r =: -r_p < \cdots < -r_1 < -r_0 := 0$ and p a positive integer, $A^{(k)} \in \mathbb{C}^{d\times d}$ for $k = 0, 1, \ldots, p$ and $B^{(k)} : [-r_k, -r_{k-1}] \to \mathbb{C}^{d\times d}$ for $k = 1, \ldots, p$ sufficiently smooth. We therefore assume that

$$\mathcal{M}\phi = \sum_{k=1}^{p} \mathcal{M}^{(k)}\phi^{(k)}, \tag{8}$$

where $\phi^{(k)}$ is the restriction of $\phi \in X$ to the kth delay subinterval $[-r_k, -r_{k-1}]$:

$$\begin{aligned} \mathcal{M}^{(1)}\phi^{(1)} &= -C_1\phi^{(1)}(0) - C_2(\phi^{(1)})'(0) \\ &\quad + A^{(0)}\phi^{(1)}(0) + A^{(1)}\phi^{(1)}(-r_1) + \int_{-r_1}^{0} B^{(1)}(\theta)\phi^{(1)}(\theta)\,\mathrm{d}\theta \end{aligned} \tag{9}$$

and, for $k = 2, \ldots, p$,

$$\mathcal{M}^{(k)}\phi^{(k)} = A^{(k)}\phi^{(k)}(-r_k) + \int_{-r_k}^{-r_{k-1}} B^{(k)}(\theta)\phi^{(k)}(\theta)\,\mathrm{d}\theta. \tag{10}$$

3. IG approach

In this section, we approximate a finite number of the eigenvalues of the IG $\mathcal{A}$ defined in Equation (6) through the eigenvalues of a matrix $\mathcal{A}_N$ that constitutes a discrete approximation of $\mathcal{A}$. We extend to systems of coupled VFEs and DDEs (3) the pseudospectral scheme developed in [2] for DDEs, where the domain condition is specified through $\phi'(0)$, by combining it with the different strategy adopted in [5], where the domain condition is specified through $\phi(0)$. We first present the method for Equation (6) with a general $\mathcal{M}$ piecewise defined as in Equation (8). Then, a concrete algorithm is given for $\mathcal{M}$ such that Equations (5) and (7) apply.

For a given set of possibly different positive integers $\{N_k,\ k=1,\dots,p\}$, define $N := \sum_{k=1}^{p} N_k$ and introduce on the interval $[-r,0]$ the piecewise mesh $\Omega_N := \bigcup_{k=1}^{p} \Omega_{N_k}^{(k)}$, where $\Omega_{N_k}^{(k)}$ is the mesh of N_k+1 distinct nodes on $[-r_k,-r_{k-1}]$ given by

$$\Omega_{N_k}^{(k)} := \left\{ \theta_i^{(k)},\ i=0,1,\dots,N_k : -r_k = \theta_{N_k}^{(k)} < \cdots < \theta_0^{(k)} = -r_{k-1} \right\}.$$

Note that $\theta_0^{(k+1)} = \theta_{N_k}^{(k)}$ for $k=1,\dots,p-1$. Let $X_N := (\mathbb{C}^d)^{\Omega_N \setminus \{0\}} \cong \mathbb{C}^{dN}$. The 'discretization map' sends $\phi \in X$ to the dN-vector

$$x_N = (x_1^{(1)},\dots,x_{N_1}^{(1)},x_1^{(2)},\dots,x_{N_2}^{(2)},\dots,x_1^{(p)},\dots,x_{N_p}^{(p)})^{\mathrm{T}} \in X_N, \tag{11}$$

where $x_i^{(k)} = \phi(\theta_i^{(k)}) \in \mathbb{C}^d$, $i=1,\dots,N_k$, $k=1,\dots,p$. Because i does not take the value 0, common boundary points of subintervals are represented only once, yet we set also $x_0^{(k+1)} := x_{N_k}^{(k)}$ to reflect $\theta_0^{(k+1)} = \theta_{N_k}^{(k)}$ for $k=1,\dots,p-1$.

Given a vector $x_N \in X_N$, let ϕ_N be the piecewise polynomial defined on $[-r,0]$ by the following conditions:

(i) ϕ_N is continuous;
(ii) ϕ_N is an N_k-degree polynomial $\phi_{N_k}^{(k)}$ on the interval $[-r_k,-r_{k-1}]$, $k=1,\dots,p$;
(iii) $\phi_N(\theta_i^{(k)}) = x_i^{(k)}$, $i=1,\dots,N_k$, $k=1,\dots,p$ and
(iv) $\mathcal{M}\phi_N = 0$.

A polynomial satisfying (i)–(iii) is piecewise represented as

$$\phi_{N_1}^{(1)}(\theta) = \ell_0^{(1)}(\theta)\phi_N(0) + \sum_{j=1}^{N_1} \ell_j^{(1)}(\theta) x_j^{(1)}, \quad \theta \in [-r_1,0],$$

$$\phi_{N_k}^{(k)}(\theta) = \sum_{j=0}^{N_k} \ell_j^{(k)}(\theta) x_j^{(k)}, \quad \theta \in [-r_k,-r_{k-1}],\ \ k=2,\dots,p,$$

where $\{\ell_j^{(k)}, j=0,1,\dots,N_k\}$ is the Lagrange basis corresponding to the nodes in $\Omega_{N_k}^{(k)}$ (see e.g. [1]).

To satisfy condition (iv), we choose

$$\phi_N(0) = -(\mathcal{M}^{(1)}\ell_0^{(1)} I_d)^{-1} \left(\sum_{j=1}^{N_1} \mathcal{M}^{(1)}\ell_j^{(1)} x_j^{(1)} + \sum_{k=2}^{p}\sum_{j=0}^{N_k} \mathcal{M}^{(k)}\ell_j^{(k)} x_j^{(k)} \right)$$

with $\mathcal{M}^{(k)}$ the components of $\mathcal{M}$ according to Equation (8). At this point, we assume that the inverse matrix in front of the right-hand side above is well defined for sufficiently large N_1.

Now, we replace the infinite-dimensional operator $\mathcal{A}$ on X by the finite-dimensional operator $\mathcal{A}_N$ on X_N defined by

$$[\mathcal{A}_N x_N]_i^{(k)} = \phi_N'(\theta_i^{(k)}), \quad i = 1, \dots, N_k, \ \ k = 1, \dots, p.$$

By setting for brevity

$$\mathcal{M}_j^{(k)} := \mathcal{M}^{(k)} \ell_j^{(k)} I_d, \quad j = 0, 1, \dots, N_k, \ \ k = 1, \dots, p, \tag{12}$$

and

$$\mathcal{D}_{ij}^{(k)} := (\ell_j^{(k)})'(\theta_i^{(k)}) I_d, \quad i, j = 0, 1, \dots, N_k, \ \ k = 1, \dots, p,$$

we get

$$\begin{aligned}[\mathcal{A}_N x_N]_i^{(1)} = &\sum_{j=1}^{N_1} (\mathcal{D}_{ij}^{(1)} - \mathcal{D}_{i0}^{(1)} (\mathcal{M}_0^{(1)})^{-1} \mathcal{M}_j^{(1)}) x_j^{(1)} \\ &+ \sum_{k=2}^{p} \sum_{j=0}^{N_k} \mathcal{D}_{i0}^{(1)} (\mathcal{M}_0^{(1)})^{-1} \mathcal{M}_j^{(k)} x_j^{(k)}, \quad i = 1, \dots, N_1,\end{aligned}$$

and

$$[\mathcal{A}_N x_N]_i^{(k)} = \sum_{j=0}^{N_k} \mathcal{D}_{ij}^{(k)} x_j^{(k)}, \quad i = 1, \dots, N_k, \ \ k = 2, \dots, p.$$

With abuse of notation, let $\mathcal{A}_N \in \mathbb{C}^{dN \times dN}$ denote also the canonical matrix representing the operator $\mathcal{A}_N : X_N \to X_N$. Note that this matrix has a special block structure according to the number and distribution of the delays. For $h, k = 1, \dots, p$, the (h, k)th block is itself a $N_h \times N_k$ block matrix with blocks of dimension $d \times d$. Roughly (i.e. except for overlapping due to the fact that $\theta_0^{(k+1)} = \theta_{N_k}^{(k)}$ for $k = 1, \dots, p-1$), such structure is diagonal plus first row. The blocks along the diagonal discretize the differentiation action of $\mathcal{A}$: this part is independent of the model coefficients $\mathcal{M}$. The first block row discretizes the boundary condition characterizing the domain of $\mathcal{A}$: this part depends on the model coefficients $\mathcal{M}$. An example is given in Figure 1 for $d = 3$, $p = 4$, $N_1 = 3$, $N_2 = 6$, $N_3 = 5$ and $N_4 = 8$; hence, the total size is 66×66.

Explicit expressions of the entries of $\mathcal{A}_N$ according to Equations (7), (9) and (10)–(12) follow:

$$\begin{aligned}\mathcal{M}_j^{(1)} = &-C_1 \ell_j^{(1)}(0) - C_2 (\ell_j^{(1)})'(0) \\ &+ A^{(0)} \ell_j^{(1)}(0) + A^{(1)} \ell_j^{(1)}(-r_1) + \int_{-r_1}^{0} B^{(1)}(\theta) \ell_j^{(1)}(\theta) \, \mathrm{d}\theta\end{aligned} \tag{13}$$

for $j = 0, 1, \dots, N_1$ and

$$\mathcal{M}_j^{(k)} = A^{(k)} \ell_j^{(k)}(-r_k) + \int_{-r_k}^{-r_{k-1}} B^{(k)}(\theta) \ell_j^{(k)}(\theta) \, \mathrm{d}\theta \tag{14}$$

for $j = 0, 1, \dots, N_k$ and $k = 2, \dots, p$. Let us remark that, in general, the distributed delay terms above cannot be calculated exactly. If this is the case, a quadrature rule must be adopted, and we resort to the piecewise interpolatory formula based on the same nodes in Ω_N. Proceeding in this

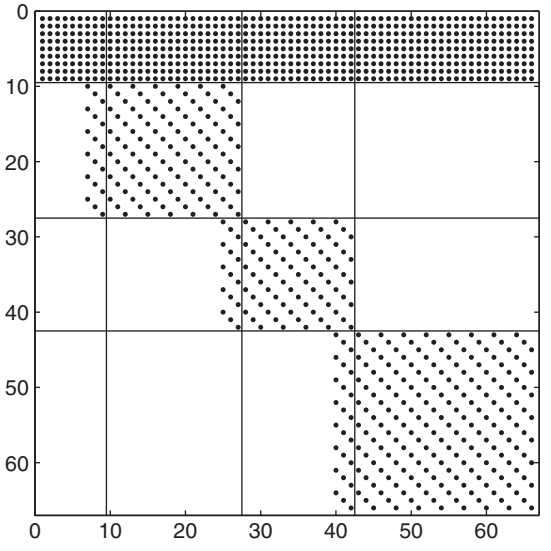

Figure 1. An example of the block structure of $\mathcal{A}_N$.

way, in fact, and thanks to the cardinal property of the Lagrange basis, that is,

$$\ell_j^{(k)}(\theta_i^{(k)}) = \delta_{ij}, \quad i,j = 0,1,\ldots,N_k, \;\; k = 1,\ldots,p,$$

with δ the Kronecker delta, one always obtains

$$\mathcal{M}_j^{(1)} = -C_1\delta_{0j} - C_2\mathcal{D}_{0j}^{(1)} + A^{(0)}\delta_{0j} + A^{(1)}\delta_{N_1 j} + \frac{r_1}{2}\omega_j^{(1)}B^{(1)}(\theta_j^{(1)}) \tag{15}$$

for $j = 0,1,\ldots,N_1$ and

$$\mathcal{M}_j^{(k)} = A^{(k)}\delta_{N_k j} + \frac{r_k - r_{k-1}}{2}\omega_j^{(k)}B^{(k)}(\theta_j^{(k)}) \tag{16}$$

for $j = 0,1,\ldots,N_k$ and $k = 2,\ldots,p$, with quadrature weights $\omega_j^{(k)}$ relevant to the scaled interval $[-1,1]$.

Algorithm 1 provides a pseudocode to build the matrix $\mathcal{A}_N$ explicitly. We use the following compact notation: $[\mathcal{A}_N]_{i_h,j_k}$ denotes the (i_h,j_k)th $(d \times d)$-block of $\mathcal{A}_N$, where $i_h := \sum_{l=1}^{h-1} N_l + i$, $i = 1,\ldots,N_h$, $h = 1,\ldots,p$, and, according to the sequential ordering (11) of the components in X_N, i_h refers to the ith mesh node inside the hth interval, that is, $\theta_i^{(h)}$. The same for j_k. Recall also the superpositions at the delay discontinuities $-r_k = \theta_{N_k}^{(k)} = \theta_0^{(k+1)}$, $k = 1,\ldots,p-1$. Some useful remarks follow:

- The computation of the inverse of $\mathcal{M}_0^{(1)}$ is a safe step since the dimension d is sufficiently low in general. If that is not the case, it is better to avoid the computation of the inverse and rather solve the corresponding linear system whenever the product with the inverse is required; for this just a single factorization of $\mathcal{M}_0^{(1)}$ is necessary.
- As mesh nodes, we advise the use of Chebyshev extremal points

$$\theta_i^{(k)} = \frac{r_k - r_{k-1}}{2}\cos\left(\frac{i\pi}{N_k}\right) - \frac{r_k + r_{k-1}}{2}, \quad i = 0,1,\ldots,N_k, \;\; k = 1,\ldots,p, \tag{17}$$

since efficient routines to compute the relevant differentiation matrices and quadrature weights

are available (see e.g. [21]). Convergence considerations given later on will motivate the choice further.

- Although any choice of $N_1, \ldots, N_p$ is admitted, interpolation considerations suggest a proportional subdivision w.r.t. the length of the delay subintervals. One possibility is, for example, to choose N and define
$$N_k = \left\lceil N \frac{r_k - r_{k-1}}{r_p} \right\rceil, \quad k = 1, \ldots, p,$$
and, to compensate for rounding, re-compute N as the sum of all the N_k.
- Matlab codes implementing Algorithm 1 are available through the authors. A first m-file *script* contains all the information about the model and can be easily compiled by the user. A second m-file *function* implements the numerical part and only requires the user to give as input N, a set of model parameters to be varied for checking robustness and the name of the previous file.

4. Results

The pseudospectral differencing method proposed in [2] for computing the eigenvalues of DDEs linearized around a given equilibrium solution has been proven to be spectrally accurate under standard regularity assumptions on the model coefficients and by choosing the Chebyshev extremal points (17) as mesh nodes [2, Theorem 3.7]. An analogous result has been proven in [5] for Gurtin–MacCamy equations [5, Theorem 5.7]. In the latter, the method of Breda *et al*. [2] has been adapted in order to take into account that the condition characterizing the domain of the IG involves $\phi(0)$ rather than $\phi'(0)$. In this work, the domain condition is mixed as expressed in Equation (5) and the developed method combines the earlier two. Therefore, by analogy with [2,5] and the results therein, we see no obstacle in extending the proof of convergence. So, we expect that, by assuming that the kernels involved in the definition of $\mathcal{M}$ are sufficiently smooth and by using Chebyshev extremal points, one can prove that if $\mathcal{A}$ has an eigenvalue $\lambda \in \mathbb{C}$ with multiplicity ν, then, for sufficiently large N, $\mathcal{A}_N$ has exactly ν eigenvalues $\lambda_i \in \mathbb{C}$ counted with their multiplicities and

$$\max_{1 \le i \le \nu} |\lambda - \lambda_i| = O\left(\left(\frac{K}{N}\right)^{N/\nu}\right) \tag{18}$$

holds with some constant K independent of N and proportional to $|\lambda|$. The tests below will provide experimental support to the statement. The computations (as well as those in Section 5) are performed with $N = 50$, a value ensuring enough accuracy, as it turns out. In the case of DDEs with discrete delays, the recent paper [24] provides an automatic choice of N guaranteeing the convergence within a given tolerance of the rightmost part of the spectrum.

As a first example, we test the performance of Algorithm 1 relative to the technique presented in [2]. Consider then the DDE

$$z'(t) = 2z(t) - ez(t-1). \tag{19}$$

According to the prototype model (3) together with Equation (7), we have $d_1 = 0$, $d = d_2 = 1$, $p = 1$, $r_1 = 1$, $A^{(0)} = 2$, $A^{(1)} = -e$ and $B^{(1)} = 0$. As can easily be verified, the associated IG has the exact rightmost eigenvalue $\lambda = 1$ with multiplicity $\nu = 2$. Figure 2 shows part of the spectrum computed with both techniques and the error in the rightmost eigenvalue. The spectral behaviour is confirmed for the new scheme, although the error constant is obviously different from the one in [2]. Notice the reaching of only half the machine precision due to the double multiplicity as predicted by Equation (18).

Algorithm 1 for matrix $\mathcal{A}_N$

given $d_1, d_2, p, r_1, \dots, r_p, A^{(0)}, A^{(1)}, \dots, A^{(p)}$ and $B^{(1)}, \dots, B^{(p)}$
set $N_1, \dots, N_p$ and $\Omega_{N_1}^{(1)}, \dots, \Omega_{N_k}^{(k)}$, i.e. all $\theta_i^{(k)}$'s and $\omega_i^{(k)}$'s
compute $d = d_1 + d_2$ and $N = \sum_{k=1}^{p} N_k$
construct $C_1 = \begin{pmatrix} I_{d_1} & 0 \\ 0 & 0 \end{pmatrix}$ and $C_2 = \begin{pmatrix} 0 & 0 \\ 0 & I_{d_2} \end{pmatrix}$
initialize $\mathcal{A}_N = \begin{pmatrix} 0 & \cdots & 0 \\ \vdots & \ddots & \vdots \\ 0 & \cdots & 0 \end{pmatrix} \in \mathbb{C}^{dN \times dN}$
for $k = 1$ to p **do**
  for $i, j = 0$ to N_k **do**
    $\mathcal{D}_{ij}^{(k)} = (\ell_j^{(k)})'(\theta_i^{(k)}) I_d$
  end for
end for
$\mathcal{M}_0^{(1)} = -C_1 - C_2 \mathcal{D}_{00}^{(1)} + A^{(0)} + \frac{r_1}{2} \omega_0^{(1)} B^{(1)}(\theta_0^{(1)})$
for $j = 1$ to $N_1 - 1$ **do**
  $\mathcal{M}_j^{(1)} = -C_2 \mathcal{D}_{0j}^{(1)} + \frac{r_1}{2} \omega_j^{(1)} B^{(1)}(\theta_j^{(1)})$
end for
$\mathcal{M}_{N_1}^{(1)} = -C_2 \mathcal{D}_{0N_1}^{(1)} + A^{(1)} + \frac{r_1}{2} \omega_{N_1}^{(1)} B^{(1)}(\theta_{N_1}^{(1)})$
for $k = 2$ to p **do**
  for $j = 0$ to $N_k - 1$ **do**
    $\mathcal{M}_j^{(k)} = \frac{r_k - r_{k-1}}{2} \omega_j^{(k)} B^{(k)}(\theta_j^{(k)})$
  end for
  $\mathcal{M}_{N_k}^{(k)} = A^{(k)} + \frac{r_k - r_{k-1}}{2} \omega_{N_k}^{(k)} B^{(k)}(\theta_{N_k}^{(k)})$
end for
for $i = 1$ to N_1 and $j = 1$ to N_1 **do**
  $[\mathcal{A}_N]_{i_1 j_1} = \mathcal{D}_{ij}^{(1)} - \mathcal{D}_{i0}^{(1)} (\mathcal{M}_0^{(1)})^{-1} \mathcal{M}_j^{(1)}$
end for
for $k = 2$ to p **do**
  for $i = 1$ to N_1 and $j = 0$ to N_k **do**
    $[\mathcal{A}_N]_{i_1 j_k} = [\mathcal{A}_N]_{i_1 j_k} + \mathcal{D}_{i0}^{(1)} (\mathcal{M}_0^{(1)})^{-1} \mathcal{M}_j^{(k)}$
  end for
end for
for $k = 2$ to p **do**
  for $i = 1$ to N_k and $j = 0$ to N_k **do**
    $[\mathcal{A}_N]_{i_k j_k} = \mathcal{D}_{ij}^{(k)}$
  end for
end for

As a second example, we consider a coupled system which exhibits neutral dynamics, that is, there are infinitely many eigenvalues in a vertical strip of the complex plane. The equations are

$$\begin{aligned} y(t) &= y(t-1) + (3-2e) \int_{-1}^{0} y(t+\theta)\,\mathrm{d}\theta + \int_{-1}^{0} z(t+\theta)\,\mathrm{d}\theta, \\ z'(t) &= 2 \int_{-1}^{0} y(t+\theta)\,\mathrm{d}\theta + \int_{-1}^{0} z(t+\theta)\,\mathrm{d}\theta. \end{aligned} \tag{20}$$

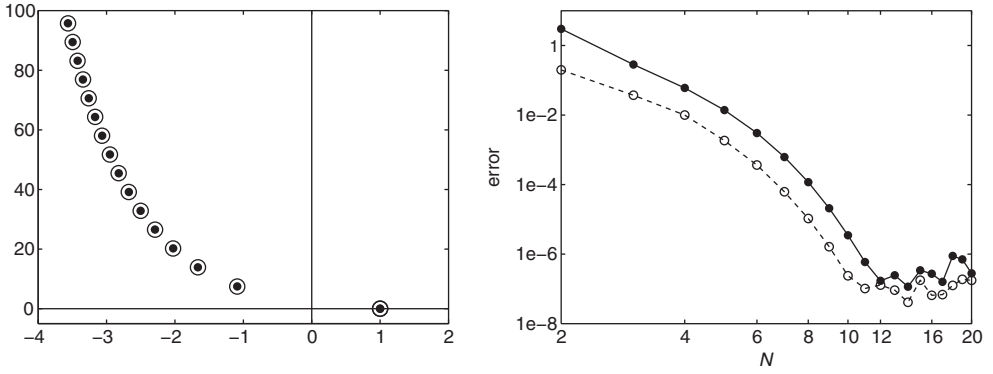

Figure 2. Computed spectrum in $\mathbb{C}$ with nonnegative imaginary part (left: • for the method in this work, ∘ for the method in [2]) and error in the computed rightmost eigenvalue (right: solid • for the method in this work, dashed ∘ for the method in [2]) for Equation (19).

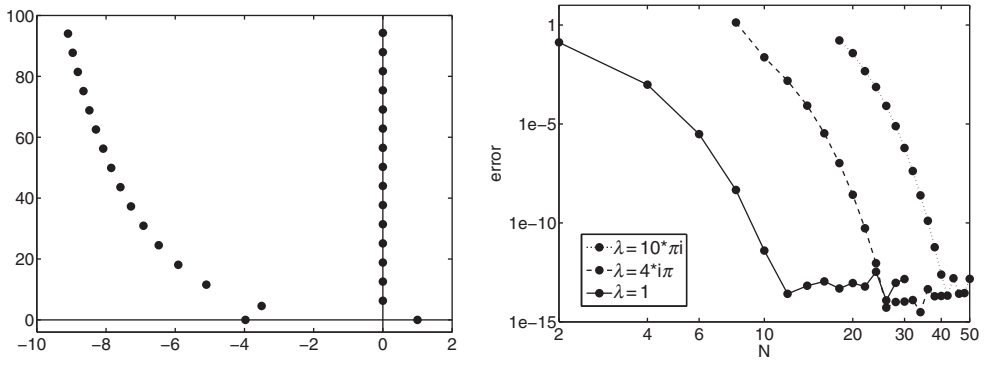

Figure 3. Computed spectrum in $\mathbb{C}$ with nonnegative imaginary part (left) and error in some eigenvalues (right) for Equation (20).

In terms of the prototype system (3) together with Equation (7), we have $d_1 = d_2 = 1$, $d = 2$, $p = 1$, $r_1 = 1$ and

$$A^{(0)} = \begin{pmatrix} 0 & 0 \\ 0 & 0 \end{pmatrix}, \quad A^{(1)} = \begin{pmatrix} 1 & 0 \\ 0 & 0 \end{pmatrix}, \quad B^{(1)} = \begin{pmatrix} 3 - 2e & 1 \\ 2 & 1 \end{pmatrix}.$$

As can easily be verified, the associated IG has the exact rightmost eigenvalue $\lambda = 1$ as well as the exact imaginary eigenvalues $\lambda = \pm 2k\pi \mathrm{i}$, $k = 1, 2, \ldots$. Figure 3 shows part of the spectrum computed with the new technique as well as the error in the rightmost and in two imaginary eigenvalues. The spectral behaviour is confirmed also w.r.t. the role of the constant K in Equation (18).

As a third example, we test the following coupled system:

$$\begin{aligned} y(t) &= y(t) + z(t) + ey(t-1) + ez(t-1), \\ z'(t) &= \frac{1}{2}y(t) + z(t) + ez(t-1). \end{aligned} \tag{21}$$

In terms of the prototype system (3) together with Equation (7), we have $d_1 = d_2 = 1$, $d = 2$, $p = 1$, $r_1 = 1$ and

$$A^{(0)} = \begin{pmatrix} 1 & 1 \\ \frac{1}{2} & 1 \end{pmatrix}, \quad A^{(1)} = \begin{pmatrix} e & e \\ 0 & e \end{pmatrix}, \quad B^{(1)} = \begin{pmatrix} 0 & 0 \\ 0 & 0 \end{pmatrix}.$$

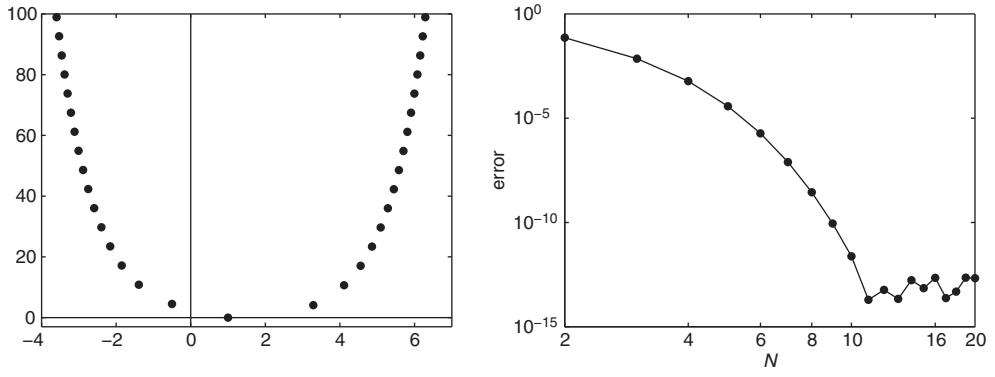

Figure 4. Computed spectrum in $\mathbb{C}$ with nonnegative imaginary part (left) and error in the eigenvalue $\lambda = 1$ (right) for Equation (21).

As can easily be verified, the associated IG has the exact eigenvalue $\lambda = 1$. Figure 4 shows again part of the computed spectrum (as well as the error in the real eigenvalue, still spectrally accurate) revealing a mixed-type dynamics, that is, infinitely many eigenvalues also in a right half-plane. Indeed, it is easy to show that z in Equation (21) satisfies the advanced–retarded scalar equation

$$z'(t) = \frac{1}{2}z(t) + ez(t-1) - \frac{1}{2e}z(t+1).$$

We refer to [3,20] for further information on the spectrum of mixed-type functional differential equations.

The tests carried out for Equations (20) and (21) show that the developed method is suitable for a class of models much wider than coupled VFEs/DDEs such as Equation (1), for which the spectrum is confined to a left-hand half of $\mathbb{C}$ with at most finitely many points in any vertical strip. The authors intend to continue the study in this direction along the lines of Breda *et al*. [3].

As a final remark, let us underline that the spectral accuracy conjectured in Equation (18) translates into very low errors for rather low matrix dimension, which in turn allows for extremely fast eigenvalue computation by standard algebraic eigensolvers (e.g. eig in Matlab). This means that a single run for a fixed choice of the model parameters and of the relevant equilibria can be efficiently repeated in order to assess the robustness. This is very helpful for producing bifurcation diagrams and detecting stability boundaries. This is the subject of Section 5, where more realistic models will be treated.

5. Applications

In this section, we perform an equilibrium stability analysis for two models of structured populations. The first is a caricatural egg cannibalism model; the second is a simplified version of the Daphnia structured consumer–resource model (1) (see e.g. [11,19]). The aim is to illustrate the efficiency and efficacy of the method as a tool to overcome the difficulties often encountered in the theoretical analysis of the characteristic equation.

5.1. *Cannibalism*

Consider the VFE

$$A(t) = \beta_0 \int_{\bar{a}}^{\infty} A(t-a)\mathcal{F}(a)\, \mathrm{e}^{-\int_0^a A(t-a+\sigma)h(\sigma)\,\mathrm{d}\sigma}\,\mathrm{d}a \tag{22}$$

modelling the time evolution of the size A of the subpopulation of adults in a population subject to the phenomenon of cannibalism. Here, $\beta_0 > 0$, $\mathcal{F}(a)$ and $\bar{a} > 0$ are, respectively, the constant reproduction rate, the survival probability till age $a \geq 0$ and the maturation age; $h(a)$ is the vulnerability to cannibalism of juveniles at age a with h having support in $[0, \bar{a}]$. As a caricature, we consider

$$h(a) = \begin{cases} \dfrac{c}{\epsilon} & \text{if } 0 \leq a \leq \epsilon, \\ 0 & \text{if } a \geq \epsilon, \end{cases}$$

in the limit $\epsilon \to 0$ and

$$\mathcal{F}(a) = \begin{cases} \mathcal{F}(\bar{a}) & \text{if } \bar{a} \leq a \leq a_{\max}, \\ 0 & \text{if } a \geq a_{\max}, \end{cases} \tag{23}$$

for given and positive c, $\mathcal{F}(\bar{a})$ and $a_{\max} > \bar{a}$. By setting $\beta := \beta_0 \mathcal{F}(\bar{a})$ and after scaling A so that we can assume $c = 1$, Equation (22) reads

$$A(t) = \beta \int_{\bar{a}}^{a_{\max}} A(t-a)\, \mathrm{e}^{-A(t-a)} \mathrm{d}a. \tag{24}$$

Equation (24) possesses always the trivial equilibrium $\bar{A}_0 = 0$. The nontrivial equilibrium

$$\bar{A}_1 = \log\left[\beta(a_{\max} - \bar{a})\right]$$

is biologically meaningful iff

$$\beta(a_{\max} - \bar{a}) > 1. \tag{25}$$

We are interested in the stability of the equilibria for a given fixed $a_{\max}$ and for varying β and $\bar{a}$. The above choices allow for an exact analysis, so that we can eventually verify the correctness of the IG approach by computing the eigenvalues for any choice of the parameters.

The linearization of Equation (24) around $\bar{A}_1$ leads to

$$y(t) = \frac{1 - \log\left[\beta(a_{\max} - \bar{a})\right]}{a_{\max} - \bar{a}} \int_{\bar{a}}^{a_{\max}} y(t-a)\, \mathrm{d}a, \tag{26}$$

which is of the form (3) together with Equation (7) with $d = d_1 = 1$, $d_2 = 0$, $p = 2$, $r_1 = \bar{a}$, $r_2 = a_{\max}$, $A^{(0)} = A^{(1)} = A^{(2)} = B^{(1)} = 0$ and

$$B^{(2)} = \frac{1 - \log\left[\beta(a_{\max} - \bar{a})\right]}{a_{\max} - \bar{a}}.$$

The associated characteristic equation reads

$$1 = \frac{1 - \log\left[\beta(a_{\max} - \bar{a})\right]}{a_{\max} - \bar{a}} \cdot \frac{\mathrm{e}^{-\lambda \bar{a}} - \mathrm{e}^{-\lambda a_{\max}}}{\lambda}.$$

By letting $\lambda = \mathrm{i}\omega$, we get the two real equations

$$\begin{aligned} \cos(\omega \bar{a}) &= \cos(\omega a_{\max}), \\ \omega &= \frac{1 - \log\left[\beta(a_{\max} - \bar{a})\right]}{a_{\max} - \bar{a}} \cdot \left[\sin(\omega a_{\max}) - \sin(\omega \bar{a})\right], \end{aligned}$$

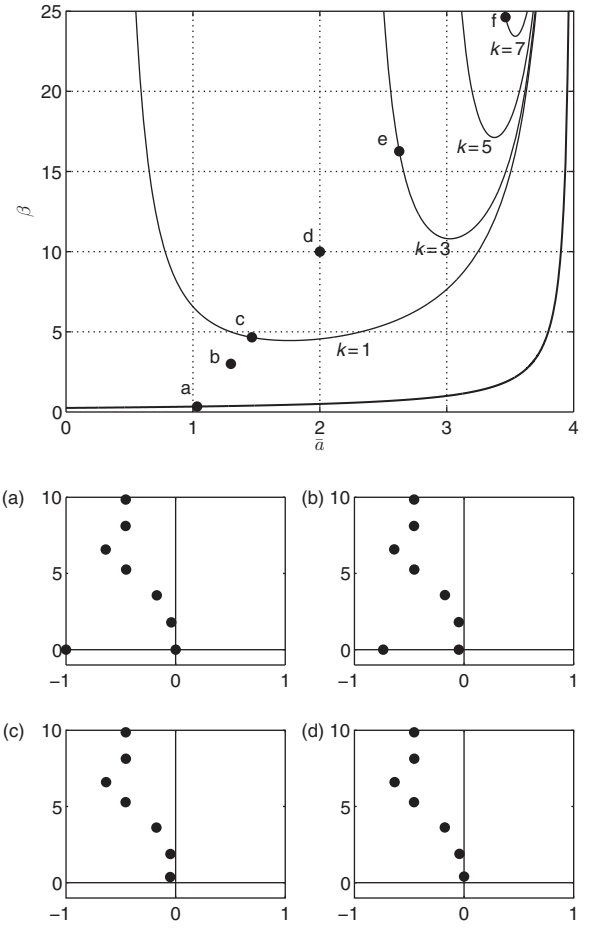

Figure 5. Stability regions (top) in the plane $(\bar{a}, \beta)$ for the equilibria of Equation (24) for $a_{\max} = 4$; corresponding eigenvalues in $\mathbb{C}$ with nonnegative imaginary part (bottom) for some choices of $\bar{a}$ and β.

which can be rearranged to get the following set for $k = 1, 3, 5, \ldots$ of parametric curves in the plane $(\bar{a}, \beta)$, parametrized by ω, with $\omega \geq 0$ for symmetry reasons, for a given $a_{\max}$:

$$\beta = \frac{1}{2(a_{\max} - k\pi/\omega)} \mathrm{e}^{1-(\omega a_{\max} - k\pi)/\sin(\omega a_{\max})},$$
$$\bar{a} = \frac{2k\pi}{\omega} - a_{\max}.$$

Such curves are depicted in Figure 5 (solid thin) together with the curve

$$\beta = \frac{1}{a_{\max} - \bar{a}} \tag{27}$$

delimiting the region of positivity of the nontrivial equilibrium $\bar{A}_1$ (solid thick); for choices of the parameters $\bar{a}$ and β below this curve, only the trivial equilibrium $\bar{A}_0$ is meaningful and is asymptotically stable. For parameters on this curve, the rightmost eigenvalue is $\lambda = 0$ (Figure 5(a)) and when the curve is crossed the nontrivial equilibrium $\bar{A}_1$ becomes positive and is asymptotically stable (Figure 5(b)). Crossing the first thin curve upwards (solid thin, $k = 1$), a complex-conjugate

pair of eigenvalues crosses the imaginary axis from left to right, the equilibrium becomes unstable and a periodic solution arises (Figure 5(c) and (d)): a Hopf bifurcation. Every time that a thin curve is crossed upwards for increasing k, another complex pair crosses the imaginary axis (Figure 5(e) and (f)). The curve corresponding to $k = 2m + 1$ is characterized by m complex pairs on the right, one on the imaginary axis and all the others on the left. The stability analysis of the periodic solutions as well as other types of bifurcation require different tools which fall outside of the scope of this work; for those interested, see [8] as far as DDEs are concerned.

5.2. *Logistic Daphnia*

Consider the coupled system of one VFE and one DDE

$$\begin{aligned} b(t) &= \beta_0 S(t) \int_{\bar{a}}^{\infty} b(t-a)\mathcal{F}(a)\,\mathrm{d}a, \\ S'(t) &= rS(t)\left(1 - \frac{S(t)}{K}\right) - \gamma_0 S(t) \int_{\bar{a}}^{\infty} b(t-a)\mathcal{F}(a)\,\mathrm{d}a, \end{aligned} \tag{28}$$

which is a special and simplified version of Equation (1). $\beta_0 > 0$, $\gamma_0 > 0$, $\mathcal{F}(a)$ and $\bar{a} > 0$ are, respectively, the constant reproduction rate of adults, the consumption rate, the survival probability till age $a \geq 0$ and the maturation age of the consumer. $r > 0$ and $K > 0$ are, respectively, the constant reproduction rate and the carrying capacity of the resource. Let us choose $\mathcal{F}$ as in Equation (23) and set $\beta := \beta_0 \mathcal{F}(\bar{a})$ and $\gamma := \gamma_0 \mathcal{F}(\bar{a})$ so that Equation (28) becomes

$$\begin{aligned} b(t) &= \beta S(t) \int_{\bar{a}}^{a_{\max}} b(t-a)\,\mathrm{d}a, \\ S'(t) &= rS(t)\left(1 - \frac{S(t)}{K}\right) - \gamma S(t) \int_{\bar{a}}^{a_{\max}} b(t-a)\,\mathrm{d}a. \end{aligned} \tag{29}$$

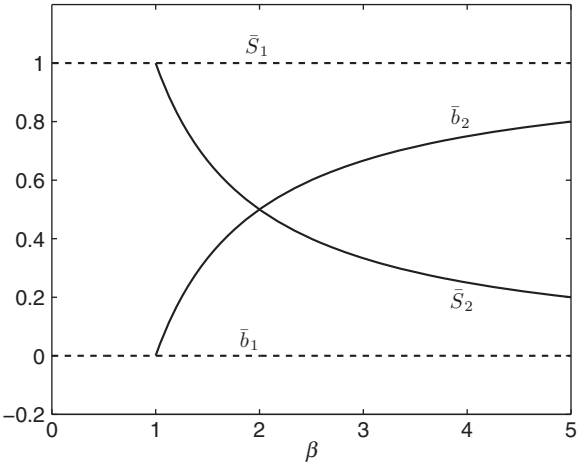

Figure 6. Equilibria E_1 (dashed) and E_2 (solid) of Equation (29) as a function of β for $r = K = \gamma = 1$, $\bar{a} = 3$ and $a_{\max} = 4$.

The possible equilibria $E = (\bar{b}, \bar{S})$ are $E_0 = (0, 0)$, $E_1 = (0, K)$ and

$$E_2 = \left(\frac{r}{\gamma(a_{\max} - \bar{a})} \left(1 - \frac{1}{K\beta(a_{\max} - \bar{a})} \right), \frac{1}{\beta(a_{\max} - \bar{a})} \right).$$

The latter is biologically meaningful iff

$$\beta \geq \frac{1}{K(a_{\max} - \bar{a})} \tag{30}$$

(Figure 6).

The linearized system reads

$$\begin{aligned} y(t) &= \beta \bar{b} z(t)(a_{\max} - \bar{a}) + \beta \bar{S} \int_{\bar{a}}^{a_{\max}} y(t-a)\, \mathrm{d}a, \\ z'(t) &= rz(t) \left(1 - 2\frac{\bar{S}}{K} \right) - \gamma z(t) \bar{b}(a_{\max} - \bar{a}) - \gamma \bar{S} \int_{\bar{a}}^{a_{\max}} y(t-a)\, \mathrm{d}a, \end{aligned} \tag{31}$$

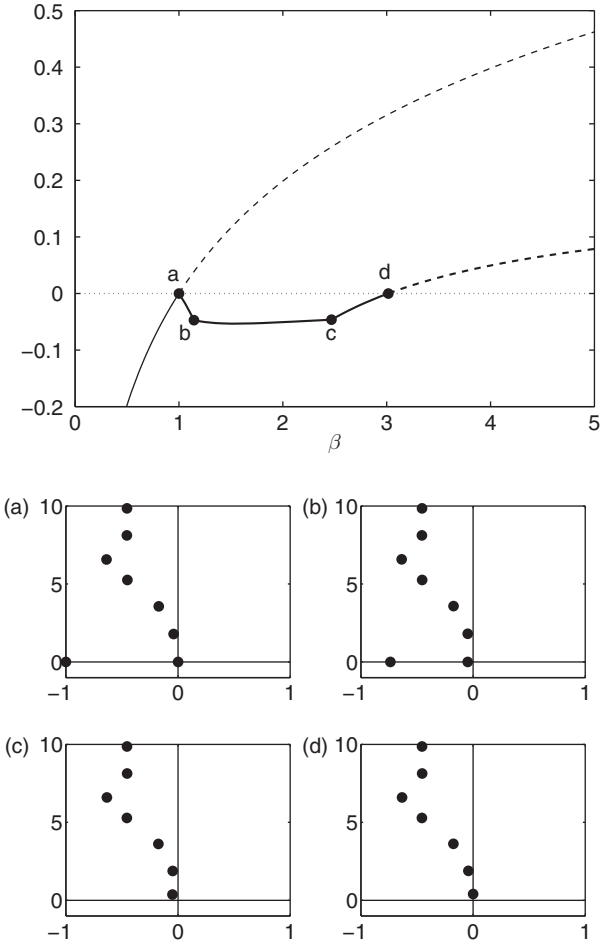

Figure 7. Real part of the rightmost eigenvalue (top panel) for the equilibria E_1 (thin) and E_2 (thick) of Equation (29) as a function of β for $r = K = \gamma = 1$, $\bar{a} = 3$ and $a_{\max} = 4$ (solid = stable, dashed = unstable); corresponding eigenvalues for E_1 (panel (a)) and for E_2 (panels (b)–(d)) in $\mathbb{C}$ with nonnegative imaginary part for the choices of β indicated by (a)–(d) in the top panel.

which is of the form (3) together with Equation (7) with $d_1 = d_2 = 1$, $d = 2$, $p = 2$, $r_1 = \bar{a}$, $r_2 = a_{\max}$

$$A^{(0)} = \begin{pmatrix} 0 & \beta\bar{b}(a_{\max} - \bar{a}) \\ 0 & r\left(1 - 2\dfrac{\bar{S}}{K}\right) - \gamma\bar{b}(a_{\max} - \bar{a}) \end{pmatrix},$$

$A^{(1)} = A^{(2)} = B^{(1)} = 0$ and

$$B^{(2)} = \begin{pmatrix} \beta\bar{S} & 0 \\ -\gamma\bar{S} & 0 \end{pmatrix}.$$

The associated characteristic equation is

$$\left[\lambda - r\left(1 - 2\frac{\bar{S}}{K}\right)\right] \cdot \left[1 - \beta\bar{S}\frac{e^{-\lambda\bar{a}} - e^{-\lambda a_{\max}}}{\lambda}\right] + \gamma\bar{b}(a_{\max} - \bar{a}) = 0. \tag{32}$$

It is easy to show that the trivial equilibrium E_0 is always unstable. A bit more effort is required to show that the equilibrium E_1 is asymptotically stable as long as

$$\beta < \frac{1}{K(a_{\max} - \bar{a})}$$

and unstable otherwise. The analysis of Equation (32) for the nontrivial equilibrium E_2 is prohibitive in general, so that we resort to the numerical computation of the eigenvalues for any fixed choice of the various model parameters r, K, β, γ, $\bar{a}$ and $a_{\max}$. Figure 7 shows the real part of the rightmost eigenvalue for the equilibria E_1 and E_2 as a function of β. As for E_1, the numerical computation of the eigenvalues confirms the theoretical findings (Figure 7(a)). As for E_2, the technique shows that it is asymptotically stable up to the value $\beta \approx 3.0162$ (numerically determined by using the IG technique), when a complex pair crosses the imaginary axis from left to right presumably giving rise to a periodic solution through a Hopf bifurcation (Figure 7(d)). Also exchanges in the rightmost eigenvalue(s) are shown (Figure 7(b) and (c)): in the transition from panel (b) to (c) for increasing β the two real eigenvalues in (b) collapse into a double real one and then split into the (lowest) complex pair in (c). This pair keeps moving rightwards causing the Hopf bifurcation in (d). This phenomenon is often observed, as described in detail in [4]. As

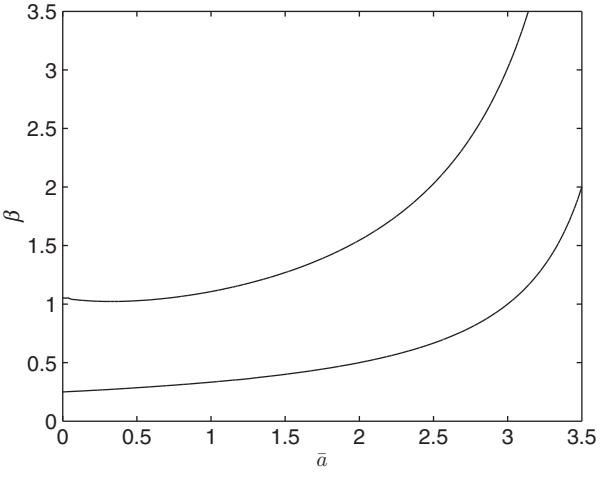

Figure 8. Existence (above the lower curve) and stability region (below the upper curve) of the equilibria E_2 of the logistic Daphnia model (29) in the plane $(\bar{a}, \beta)$ for $r = K = \gamma = 1$ and $a_{\max} = 4$.

a final example of the flexibility and efficiency of the numerical computation of the eigenvalues, we show in Figure 8 the region of asymptotic stability of the nontrivial equilibrium E_2 in the plane $(\bar{a}, \beta)$. Both curves are computed numerically by combining the computation of the real part of the rightmost eigenvalue with the algorithm in [6]. The lower curve coincides with the bound (30) and delimits the region of positivity of E_2. The upper curve is the locus of the first Hopf bifurcation: crossing the curve for increasing β, the equilibrium E_2 loses its stability and presumably a periodic solution arises.

References

[1] J.P. Berrut and L.N. Trefethen, *Barycentric Lagrange interpolation*, SIAM Rev. 46 (2004), pp. 501–517.
[2] D. Breda, S. Maset, and R. Vermiglio, *Pseudospectral differencing methods for characteristic roots of delay differential equations*, SIAM J. Sci. Comput. 27 (2005), pp. 482–495.
[3] D. Breda, S. Maset, and R. Vermiglio, *Pseudospectral approximation of eigenvalues of derivative operators with non-local boundary conditions*, Appl. Numer. Math. 56 (2006), pp. 318–331.
[4] D. Breda, C. Cusulin, M. Iannelli, S. Maset, and R. Vermiglio, *Stability analysis of age-structured population equations by pseudospectral differencing methods*, J. Math. Biol. 54 (2007), pp. 701–720.
[5] D. Breda, M. Iannelli, S. Maset, and R. Vermiglio, *Stability analysis of the Gurtin-MacCamy model*, SIAM J. Numer. Anal. 46 (2008), pp. 980–995.
[6] D. Breda, S. Maset, and R. Vermiglio, *An adaptive algorithm for efficient computation of level curves of surfaces*, Numer. Algorithms 52 (2009), pp. 605–628.
[7] D. Breda, S. Maset, and R. Vermiglio, *Numerical approximation of characteristic values of partial retarded functional differential equations*, Numer. Math. 113 (2009), pp. 181–242.
[8] D. Breda, S. Maset, and R. Vermiglio, *Approximation of eigenvalues of evolution operators for linear retarded functional differential equations*, SIAM J. Numer. Anal. 50 (2012), pp. 1456–1483.
[9] O. Diekmann, S.A. van Gils, S.M. Verduyn Lunel, and H.O. Walther, *Delay Equations – Functional, Complex and Nonlinear Analysis*, Springer-Verlag, New York, 1995.
[10] O. Diekmann, P. Getto, and M. Gyllenberg, *Stability and bifurcation analysis of Volterra functional equations in the light of suns and stars*, SIAM J. Math. Anal. 39 (2007), pp. 1023–1069.
[11] O. Diekmann, M. Gyllenberg, J.A.J. Metz, S. Nakaoka, and A.M. de Roos, *Daphnia revisited: Local stability and bifurcation theory for physiologically structured population models explained by way of an example*, J. Math. Biol. 61 (2010), pp. 277–318.
[12] K. Engelborghs, T. Luzyanina, and D. Roose, *Numerical bifurcation analysis of delay differential equations using DDE-BIFTOOL*, ACM Trans. Math. Softw. 28 (2002), pp. 1–21.
[13] A. Franceschetti, A. Pugliese, and D. Breda, *Multiple endemic states in age-structured SIR epidemic models*, Math. Biosci. Eng. 9 (2012), pp. 577–599.
[14] T. Insperger and G. Stépán, *Semi-discretization for Time-Delay Systems – Stability and Engineering Applications*, Springer-Verlag, New York, 2011.
[15] K. Ito and F. Kappel, *The Trotter–Kato theorem and approximation of PDEs*, Math. Comp. 67 (1998), pp. 21–44.
[16] T. Kato, *Perturbation Theory for Linear Operators*, Springer-Verlag, Berlin, 1976.
[17] N. Olgac and R. Sipahi, *An exact method for the stability analysis of time delayed LTI systems*, IEEE Trans. Automat. Control 47 (2002), pp. 793–797.
[18] A.M. de Roos and L. Persson, *Population and Community Ecology of Ontogenetic Development*, Princeton University Press, Princeton, NJ, 2013.
[19] A.M. de Roos, O. Diekmann, P. Getto, and M.A. Kilionis, *Numerical equilibrium analysis for structured consumer resource models*, Bull. Math. Biol. 72 (2010), pp. 259–297.
[20] A. Rustichini, *Functional differential equations of mixed type: The linear autonomous case*, J. Dynam. Differential Equations 1 (1989), pp. 121–143.
[21] L.N. Trefethen, *Spectral Methods in MATLAB*, SIAM, Philadelphia, PA, 2000.
[22] T. Vyhlídal and P. Zítek, *Mapping based algorithm for large-scale computation of quasi-polynomial zeros*, IEEE Trans. Automat. Control 54 (2009), pp. 171–177.
[23] J.H. Wilkinson, *The perfidious polynomial*, in *Studies in Numerical Analysis*, Studies in Mathematics, Vol. 24, Gene H. Golub, ed., Mathematical Association of America, Washington, DC, 1984, pp. 1–28.
[24] Z. Wu and W. Michiels, *Reliably computing all characteristic roots of delay differential equations in a given right half plane using a spectral method*, J. Comput. Appl. Math. 236 (2012), pp. 2499–2514.